Transition metal compounds with S/N-functionalized NHC ligands: structures, redox properties and electrocatalytic activity

Luo, S.; Luo S.

APPENDIX I

Setup used for the quantification of dihydrogen evolution
and equations for the determination of overpotentials

I.1. CPE-GC setup for the quantification of dihydrogen evolution

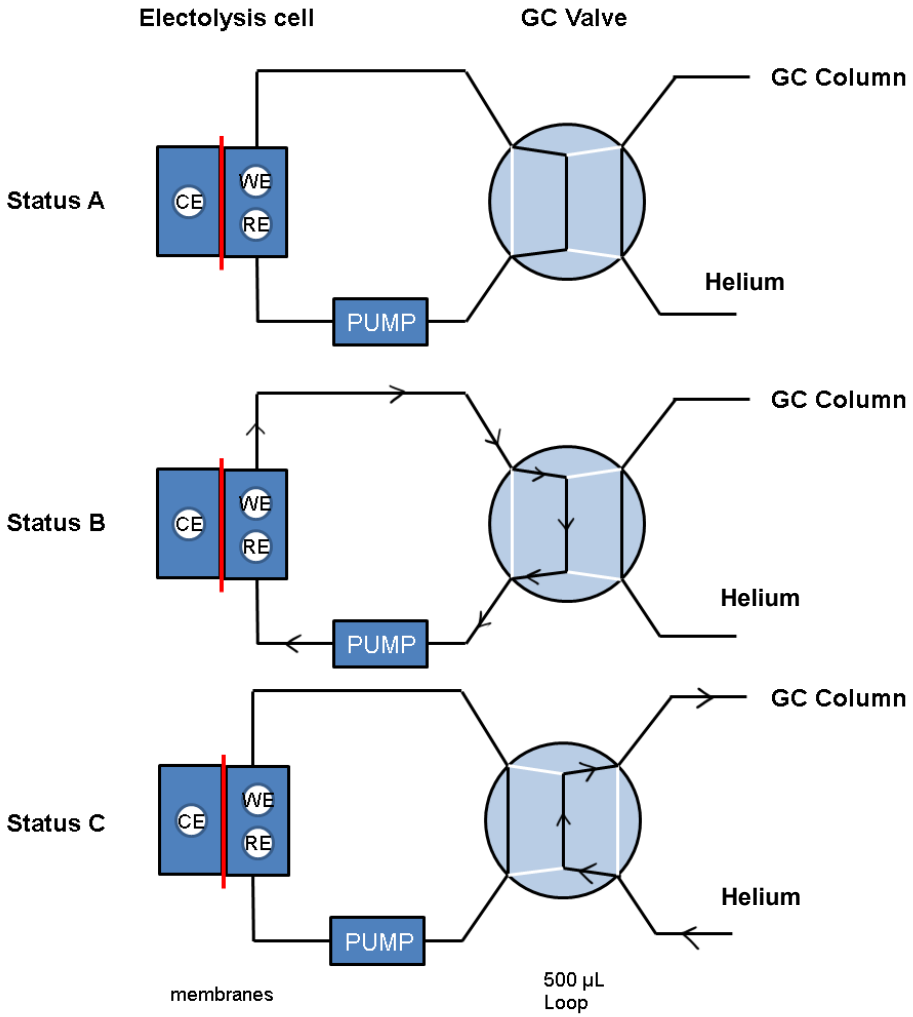

Figure AI.1. Schematic drawing of the CPE-GC setup for H_2 quantification. CE = counter electrode, WE = working electrode, RE = reference electrode; for explanation see text.

Dihydrogen evolution was measured using the setup schematically depicted in Figure AI.1. The whole setup mainly consists of three parts: the electrolysis cell, a GC valve and a GC column. The electrolysis cell is a two chamber cell separated by Nafion membranes. The counter electrode is placed in one chamber; the working electrode and reference electrode are placed in the other chamber. The chamber containing the working electrode is connected to the GC valve and contains a stir bar and 5 mL of the sample to be investigated. A pump is set between the electrochemical cell and the GC valve to circulate the helium

carrier gas. To ensure minimal leakage of air and gases, polyether ether ketone (PEEK) tubing was used for all connections between the cell, pump and GC valve.

I.2. Dihydrogen evolution measurements

Before starting the measurement, the headspace in the electrochemical cell was deaerated by pumping it around for 10 min under a constant flux of helium gas. The process of H_2 quantification can be divided into three steps: the electrolysis step, the loading step and the injection into the GC column. Firstly, the electrolysis cell is switched on and Controlled Potential Coulometry (CPC) is carried out at the selected potential (Figure AI.1 Status A). After the electrolysis experiment the potentiostat was switched off. Then the pump was turned on and the produced H_2 was delivered from the cell to a 500 μL loop (Figure AI.1 Status B). After that, the pump was switched off and the gas in the loop was delivered to a Shimadzu GC2010 fitted with a Supelco Carboxen 1010 molecular sieve column at 35 ºC using the GC valve (Figure AI.1 Status C). Helium is used as the carrier gas and the H_2 is detected using a TCD detector operated at 80 mA.

I.3. Determination of H_2 calibration line and example of dihydrogen quantification using the calibration line.

For the H_2 quantification experiments, a H_2 calibration line was made. The GC setup discussed in Section I.2 was used to make the H_2 calibration line. The electrochemical cell was fitted with the electrodes, stir bar and filled with 5 mL of the solvent. The use of an entirely identical cell setup ensures that the volume of the system is constant. Hamilton GASTIGHT® Syringes were used to take a certain volume (ranging from 40 to 800 μL) of pure H_2 which is then injected into the electrolysis cell. The gas in the cell is then measured in the GC setup following the procedure described in Section I.2. The H_2 calibration line used for the generation of the data described in this dissertation is shown in Figure AI.2. The function of the fit of the H_2 calibration line is:

$$V(H_2) = 0.01649 \times \text{Area} - 2.9941;$$

Taking compound [Ni(**L1**)]Cl in Chapter 5 as an example for the calculation: Compound [Ni(**L1**)]Cl (2 mg) and acetic acid (24 μL) were added into 5 mL DMF containing TBAP in a concentration of 0.1 M as supporting electrolyte to make a solution that contains 1 mM catalyst and 80 mM acid. The CPC potential was set to −1.8 V vs. Ag/AgCl. After 2 hours of electrolysis GC analysis resulted in a peak for H_2 with Area = 17230. Under the same conditions, for a solution containing the acid but in the absence of catalyst, the GC shows the Area(acid) = 6000. Thus, the volume of dihydrogen produced by the catalyst is:

$$V(H_2) = 0.01649 \times (17230 - 6000) - 2.9941 = 184.9\ \mu L$$

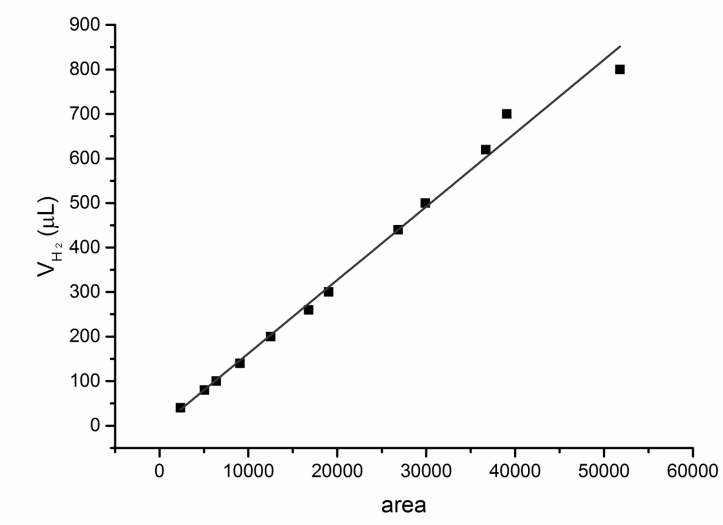

Figure AI.2. Calibration line for the quantification of H_2 using the GC setup.

I.4. Determination of the overpotential

The overpotential of a molecular electrocatalyst for H_2 production is the difference between the thermodynamic potential for the reduction of acid and the actual potential of the observed catalytic wave.[1] In this this dissertation, the half-wave potential is taken as a reference because it is both easier to obtain from the experiment and easier to compute theoretically:

$$\eta = E_{1/2}^{T} - E_{1/2}^{E} \quad (1)$$

In equation (1), $E_{1/2}^{E}$ is the experimental half-wave potential, which can be obtained from the potential of the maximum of the first derivative of the forward scan of stationary cyclic voltammograms and subtracting 15 mV.[2] $E_{1/2}^{T}$ is the thermodynamic standard potential computed in the case of an electrochemically reversible process taking into account the homoconjugation effect given by equation (2).[2]

$$E_{1/2}^{T} = E_{\mathrm{H^+/H_2}}^{\circ} - \frac{2.303 \times RT}{F} \mathrm{p}K_a + \varepsilon_D - \frac{RT}{2F} \ln \frac{C_0}{C_{\mathrm{H_2}}^{\circ}} \qquad (2)$$

In equation 2, F is Faraday's constant, T is 295 K, R is the universal gas constant, C_0 is the total concentration of acid. $C_{\mathrm{H_2}}^{\circ}$ is the concentration of dissolved dihydrogen corresponding to a partial pressure of 10^5 Pa. ε_D is a measure of the diffusion rate of the products with respect to that of reactant. The values of the physical-chemical constants ($E_{\mathrm{H^+/H_2}}^{\circ}$, $C_{\mathrm{H_2}}^{\circ}$ and ε_D) were taken from the literature.[2]

Taking compound [Ni(**L1**)]Cl in Chapter 5 as an example for the calculation: In DMF solution, $E^{\circ}_{\mathrm{H^+/H_2}} = -0.62\ V$ vs. $Fc^{+/0}$, $C^{\circ}_{\mathrm{H_2}} = 1.9\ mM$, $\varepsilon_D = 0.04\ V$, and p*K*a of acetic acid in DMF solution is 13.5, the acid concentration C_0 = 80 mM, which gives the value of $E^T_{1/2}$:

$$E^T_{1/2} = -0.62 - \frac{2.303 \times 8.314 \times 295}{96500} \times 13.5 + 0.04 - \frac{8.314 \times 295}{2 \times 96500} \ln \frac{80}{1.9} = -1.419\ \mathrm{V}$$

From the cyclic voltammetry of [Ni(**L1**)]Cl in presence of 80 mM acetic acid, the experimental half wave potential is obtained: $E^E_{1/2} = -2.345\ V$ vs. $Fc^{+/0}$.

Thus the overpotential is obtained: $\eta = E^T_{1/2} - E^E_{1/2} = 0.93\ \mathrm{V}$

I.5. Other equations used in this thesis

$$n(H_2)(\mathrm{mol}) = \frac{V(H_2)}{V_m}$$

$$N = \frac{Q\ (\mathrm{C})}{1.6 \times 10^{-19}(\mathrm{C})}$$

$$n(H_2)(\mathrm{mol}) = \frac{N}{N_A} \times \frac{1}{2}$$

Avogadro constant $N_A = 6.02 \times 10^{23}$, molar volume V_m = 24.465 L/mol.

References:

[1] R.M. Bullock, A.M. Appel, M.L. Helm, *Chem. Commun.* 2014, 50, 3125-3143.

[2] V. Fourmond, P.-A. Jacques, M. Fontecave, V. Artero, *Inorg. Chem.* 2010, 49, 10338-10347.

APPENDIX II

Supplementary information on Chapter 2

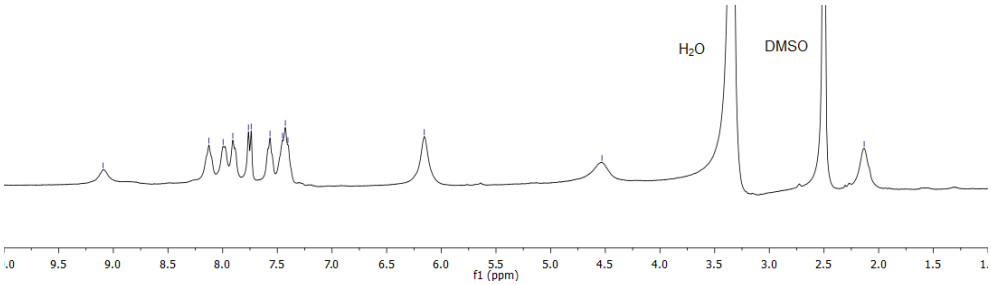

*Figure AII.1. ^{1}H NMR spectrum of complex$[Ni_2(PyC_2S)_2]Br_2$ [**3**]Br_2 in DMSO-d_6.*

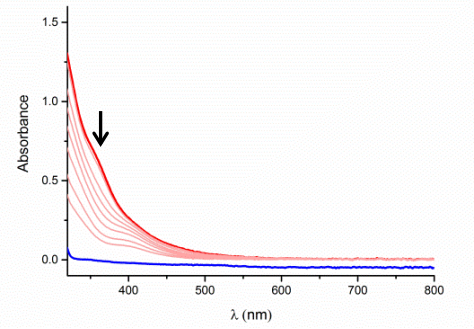

*Figure AII.2. UV-vis spectroscopic changes of a 1 mM solution of compound [**3**] in DMF in air, after addition of 210 equivalents of acetic acid in 4 h (red lines) and overnight (blue line). Spectra were recorded with a transmission dip probe set at a path length of 2.2 mm.*

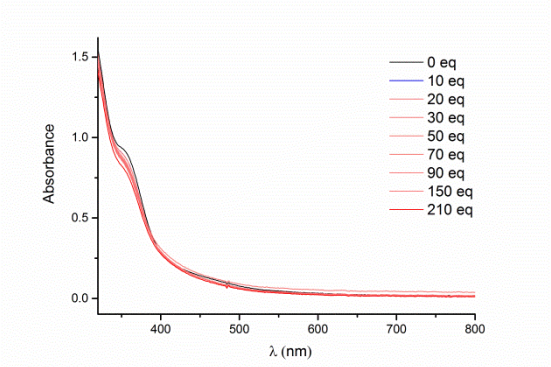

*Figure AII.3. UV-vis spectroscopic changes after sequentially adding acid (0 to 210 equivalents) into 1 mM solution of compound [**3**]Br_2 in DMF under an N_2 atmosphere. Spectra were recorded with a transmission dip probe set at a path length of 2.2 mm.*

Table AII.1. Selected crystallographic and structure refinement data for complex [1], [2], [3]Br_2 and [4]Br_2

	[1]	**[2]**	**[3]**Br_2	**[4]**Br_2
Empirical formula	$C_{32}H_{30}N_4Ni_2S_2Cl_2$	$C_{34}H_{34}N_4Ni_2S_2Cl_2$, $2(CH_2Cl_2)$	$4(C_{30}H_{28}N_6Ni_2S_2Br_2)$, CH_3OH	$C_{32}H_{32}N_6Ni_2S_2Br_2$, H_2O
Formula weight	723.04	920.94	3287.81	860.01
Temperature (K)	110(2)	110(2)	110(2)	110(2)
Crystal system	triclinic	monoclinic	monoclinic	monoclinic
Space group	*P −1*	*C 2/c*	*P 21/c*	*C 2/c*
a (Å)	8.9583(6)	31.5940(7)	27.8967(7)	30.7978(18)
b (Å)	12.2922(6)	8.77402(14)	19.0838(3)	12.2424(4)
c (Å)	13.9276(5)	31.5044(7)	29.1772(8)	21.0829(11)
α (°)	89.367(3)	90	90	90
β (°)	84.431(4)	116.465(3)	118.293(3)	121.879(7)
γ (°)	79.089(5)	90	90	90
V (Å^3)	1498.79(14)	7818.0(3)	13677.5(6)	6750(7)
Z	2	8	4	8
D_{calc} (g/cm^3)	1.602	1.565	1.597	1.693
μ (mm^{-1})	4.741	6.277	5.488	5.606
F (000)	744	3776	6600	3472
Crystal size (mm)	0.28× 0.11 × 0.05	0.40 × 0.08 × 0.05	0.24 × 0.13 × 0.02	0.11 × 0.07 × 0.06
Unique Reflections	15862	7687	26679	10502
R-factor, $I > 2\sigma(I)$	$R_1 = 0.0561$, $wR_2 = 0.1524$	$R_1 = 0.0333$, $wR_2 = 0.0814$	$R_1 = 0.0571$, $wR_2 = 0.1526$	$R_1 = 0.0484$, $wR_2 = 0.1111$
R-factor (all data)	$R_1 = 0.0619$, $wR_2 = 0.1588$	$R_1 = 0.0413$, $wR_2 = 0.0867$	$R_1 = 0.0733$, $wR_2 = 0.1662$	$R_1 = 0.0748$, $wR_2 = 0.1188$
$\Delta\rho_{max}$, $\Delta\rho_{min}$ (e Å^{-3})	0.95,−0.84	0.87, −0.61	1.93, −1.15	0.82, −0.88

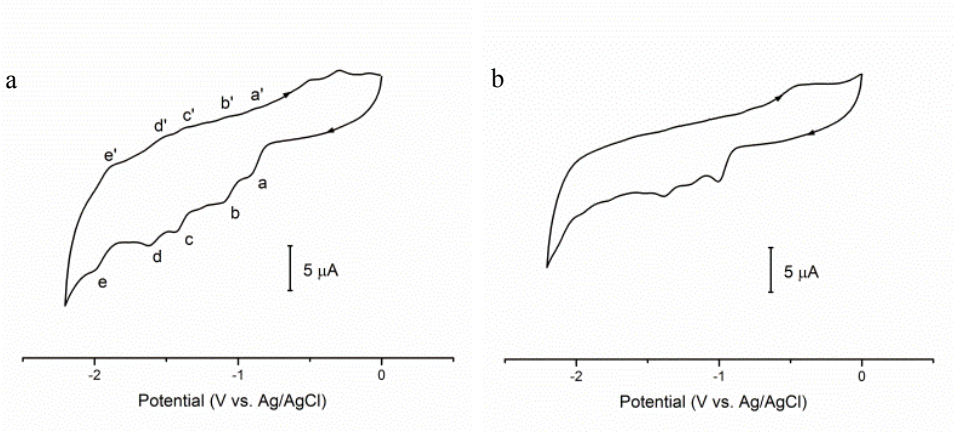

*Figure AII.4. The CV of complex [**3**]Br_2 (a) and [**4**]Br_2 (b) recorded in DMF containing 0.1 M TBAP as supporting electrolyte at scan rate 0.1 V/s, using a glassy carbon working electrode.*

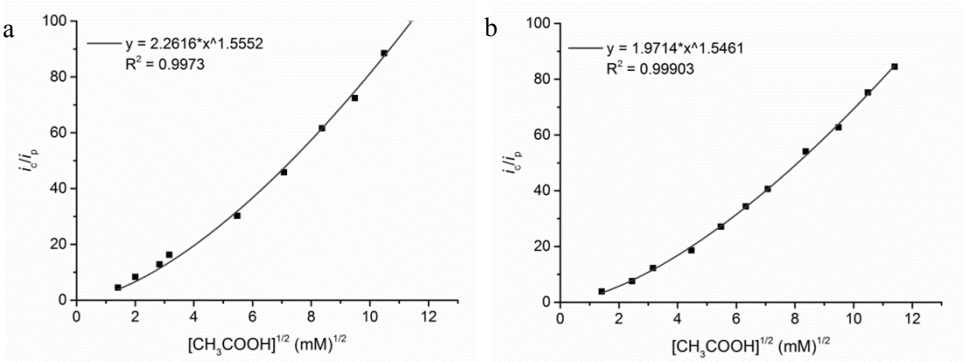

*Figure AII.5. Plot of i_c/i_p vs. $[CH_3COOH]^{1/2}$ ($mM^{1/2}$) for [**3**]Br_2 (a) and [**4**]Br_2 (b) in presence of various acid concentrations in DMF containing 0.1 M TBAP as supporting electrode at 0.1 V/s, using a glassy carbon working electrode.*

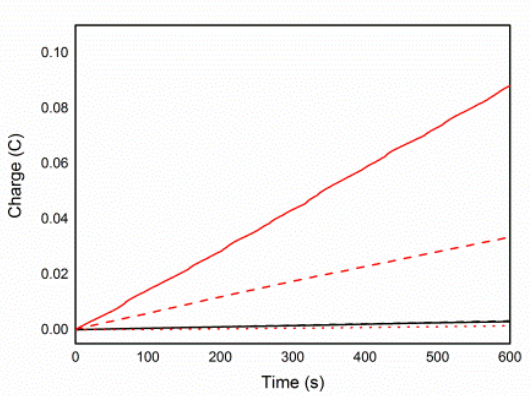

*Figure AII.6. Charge vs. time plot over 600 s during CPC at potential of −1.8 V. Black line: compounds in absence of acid; Red line: compounds in presence of 50 mM acetic acid (dashed = 1 mM $[Ni_2Cl_2(BnC_2S)_2]$ **[1]**, solid = 1mM $[Ni_2(PyC_2S)_2]Br_2$ **[3]**Br_2); Dotted red line: 50 mM acetic acid only. Using glass carbon as working electrode.*

Table AII.2. Raw data for Figure 2.10 and Figure AII.5.

***[3]**Br_2*

$[CH_3COOH]$ (mM)	$[CH_3COOH]^{1/2}$ $(mM)^{1/2}$	i_p (µA)	i_c (µA)	i_c/i_p
2	1.41	8	36	4.5
4	2	8	67	8.38
8	2.83	8	103	12.88
10	3.16	8	130	16.25
30	5.48	8	242	30.25
50	7.07	8	367	45.88
70	8.37	8	493	61.63
90	9.49	8	579	72.38
110	10.49	8	708	88.5
130	11.40	8	808	101

***[4]**Br_2*

$[CH_3COOH]$ (mM)	$[CH_3COOH]^{1/2}$ $(mM)^{1/2}$	i_p (µA)	i_c (µA)	i_c/i_p
2	1.41	8	31	3.88
6	2.45	8	61	7.63
10	3.16	8	98	12.25
20	4.47	8	149	18.63
30	5.48	8	217	27.13
40	6.32	8	275	34.38
50	7.07	8	325	40.63
70	8.37	8	433	54.13
90	9.49	8	502	62.75
110	10.49	8	602	75.25
130	11.40	8	676	84.5

APPENDIX III

Supplementary information on Chapter 3

*Table AIII.1. Selected crystallographic and structure refinement data for complexes **1a, 2a** and **2b***

	1a	**2a**	**2b**
Empirical formula	$C_{34}H_{28}BrN_6Ni$, (Br), 1.5(H_2O)	$C_{26}H_{24}N_6Ni$, 2(Br), 2.361(H_2O), 0.431(O)	$C_{26}H_{24}N_6Ni$, 2(PF_6)
Formula weight	766.18	688.50	769.16
Temperature (K)	110(2)	110(2)	110(2)
Crystal system	monoclinic	monoclinic	monoclinic
Space group	*C 2/c*	*C* 2/*c*	*P* 2_1/*c*
a (Å)	36.2037(12)	32.8374 (6),	23.0500(14)
b (Å)	11.2404(2)	8.89992 (13)	9.5940(3)
c (Å)	16.7135(6)	20.2657 (4)	14.7070(7)
β (°)	109.865(4)	109.610(2)	105.683(6)
V (Å^3)	6396.7(4)	5579.13 (18)	3131.3(3)
Z	8	8	4
D_{calc} (g/cm^3)	1.591	1.639	1.632
μ (mm^{-1})	3.145	4.65	2.796
F (000)	3096	2777	1552
Crystal size (mm)	0.27 × 0.17 × 0.10	0.26 × 0.09 × 0.02	0.25 × 0.14 × 0.01
Reflections collected, unique, $I > 2\sigma(I)$	25476, 7345, 6196	23382, 5423, 4625	18755, 6111, 5006
R-factor, $I > 2\sigma(I)$	$R_1 = 0.0290$, $wR_2 = 0.0635$	$R_1 = 0.0298$, $wR_2 = 0.0761$	$R_1 = 0.0698$, $wR_2 = 0.1823$
R-factor (all data)	$R_1 = 0.0400$, $wR_2 = 0.0674$	$R_1 = 0.0372$, $wR_2 = 0.0810$	$R_1 = 0.0832$, $wR_2 = 0.1933$
$\Delta\rho_{max}$, $\Delta\rho_{min}$ (e Å^{-3})	0.43, –0.49	0.61, –0.56	0.92, –0.71

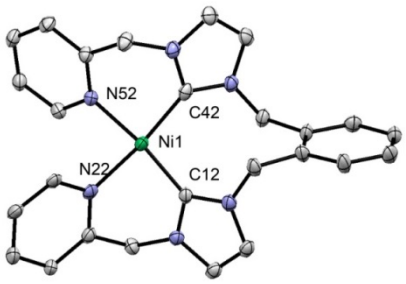

*Figure AIII.1. Displacement ellipsoid plot (50% probability level) of the cationic part [Ni(**L2**)]$^{+}$ in **2a** at 110(2) K. Selected atom numbering has been added for the first coordination sphere. Hydrogen atoms, the lattice water molecules and the two bromide anions are omitted for clarity.*

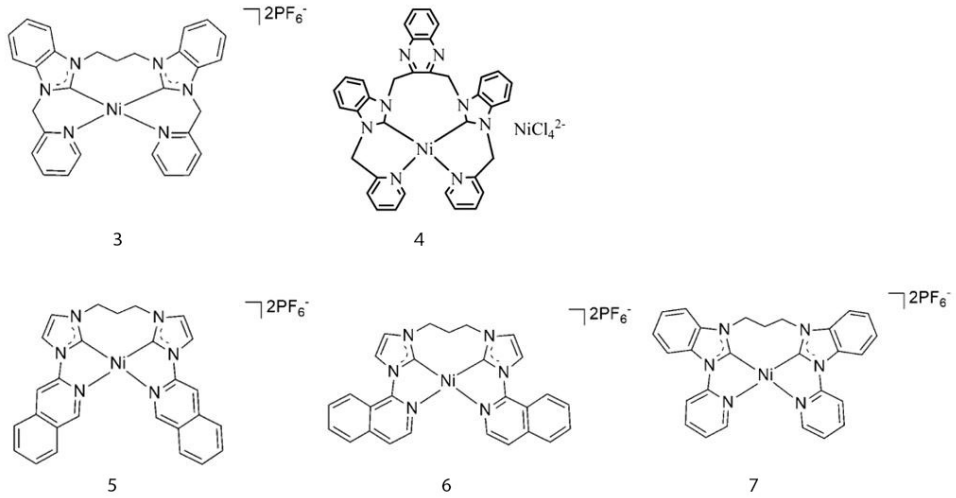

Figure AIII.2. Reported pyridinemethyl/pyridinyl/isoquinolinyl substituted Ni-NHC compounds.[1, 2]

Table AIII.2. Selected bond distances (Å) of reported Ni-NHC compounds in Figure AIII.2.

	3[a]	**4**[b]	**5**[a]	**6**[a]	**7**[a]
Ni1─N22	1.944(3)	1.945(9)	1.956(4)	1.944(1)	1.937
Ni1─N52	1.931(3)	1.945(9)	1.931(4)	1.948(1)	1.937
Ni1─C12	1.899(4)	1.883(1)	1.856(4)	1.847(1)	1.847
Ni1─C42	1.904(4)	1.883(1)	1.851(4)	1.848(2)	1.847
τ_4	0.092	0.033	0.120	0.116	0.137

[a]These complexes published by Thoi[1]. [b]These complexes published by Liu[2].

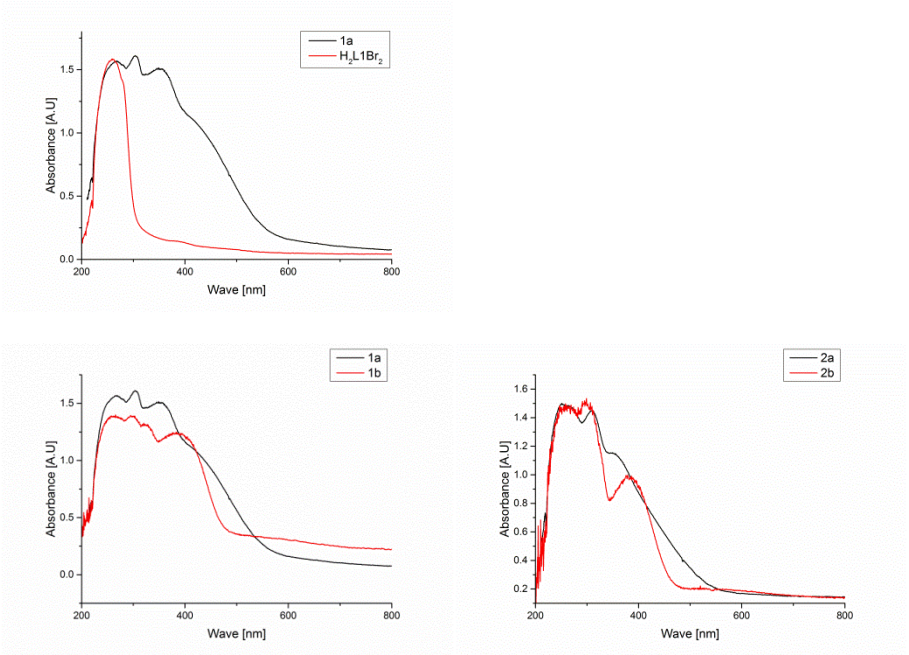

*Figure AIII.3. Solid state absorption spectra of H_2**L1**Br_2, **1a**, **1b**, **2a** and **2b**.*

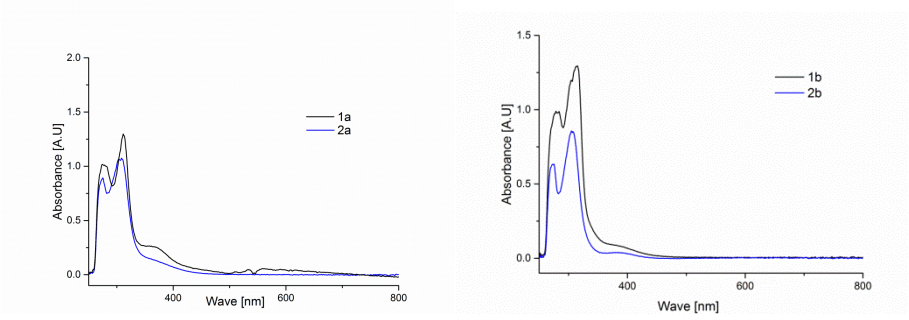

*Figure AIII.4. UV-vis spectra of **1a** (1 mM), **2a** (1 mM), **1b** (1 mM) and **2b** (1 mM) in DMF solution.*

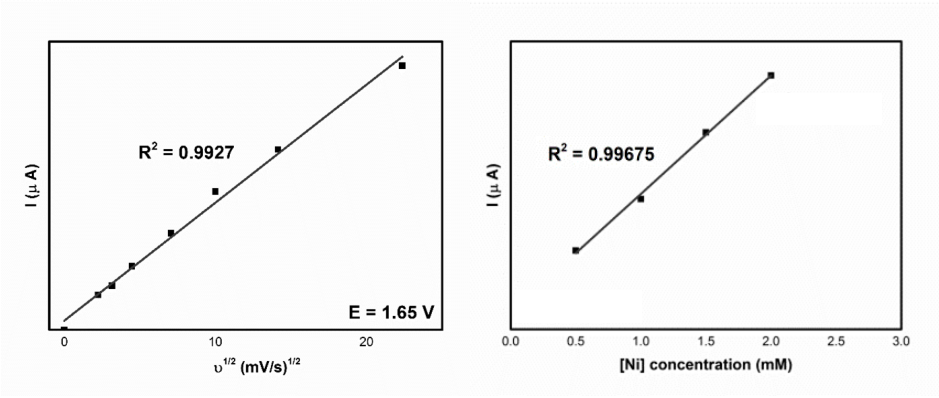

*Figure AIII.5. Plots of reductive current vs. the square root of the scan rate (right) and Plots of reductive current vs. the concentration (left) of **1a** in DMF at E = −1.65 V vs. $Fc^{+/0}$.*

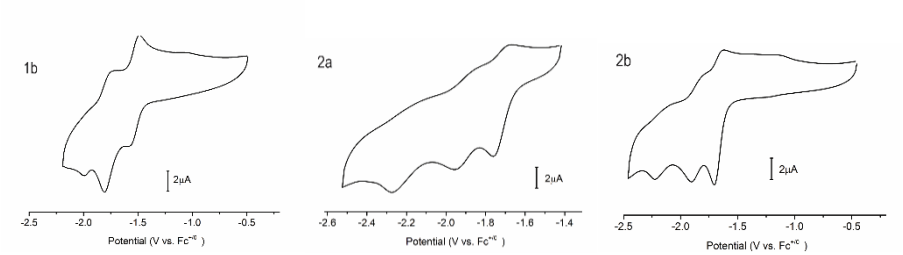

*Figure AIII.6. CV of 1 mM **1b**, **2a** and **2b** recorded in DMF. Conditions: scan rate = 0.1 V/s, TBAP (0.1 M), glassy-carbon working electrode.*

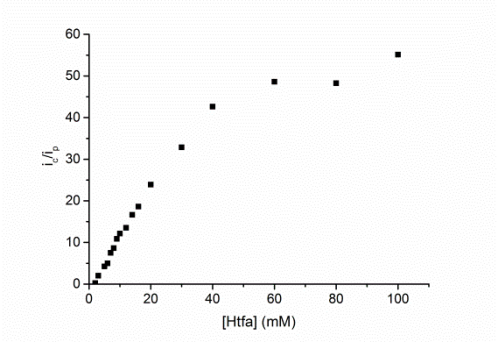

*Figure AIII.7. Plot of i_c/i_p as a function of Htfa concentration (1-100 mM) in DMF in presence of **1a** (1 mM). Conditions: scan rate = 0.1 V/s, TBAP (0.1 M), glassy-carbon working electrode.*

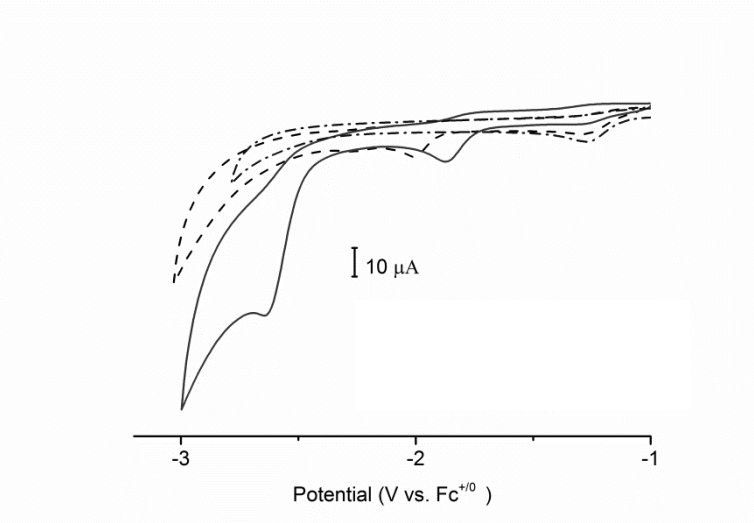

*Figure AIII.8. Cyclic voltammograms of solutions of **1a** (1 mM) (solid line) or H_2**L1**Br_2 (1 mM) (dashed line) in DMF in the presence of 10 mM acetic acid (dot-dashed line). Conditions: scan rate = 0.1V/s, TBAP (0.1 M), glassy-carbon working electrode.*

Table AIII.3. Raw data for Figure 3.4 and Figure AIII.7.

[Htfa] (mM)	$[Htfa]^{1/2}$ $(mM)^{1/2}$	i_p (µA)	i_c (µA)	i_c/i_p
2	1.41	8	2	0.25
3	1.73	8	16	2
5	2.23	8	34	4.25
6	2.45	8	40	5
7	2.66	8	60	7.5
8	2.83	8	69	8.63
9	3	8	87	10.88
10	3.16	8	97	12.13
12	3.46	8	108	13.5
14	3.74	8	133	16.63
16	4	8	149	18.63
20	4.47	8	191	23.88
30	5.48	8	263	32.88
40	6.32	8	341	42.63
60	7.75	8	389	48.63
80	8.94	8	386	48.25
100	10	8	441	55.13

Table AIII.4. Raw data for Figure 3.6 and Figure 3.7.

1a

$[CH_3COOH]$ (mM)	$[CH_3COOH]^{1/2}$ $(mM)^{1/2}$	i_p (µA)	i_c (µA)	i_c/i_p
1	1	7	40	5.71
2	1.41	7	47	6.71
4	2	7	55	7.85

6	2.45	7	61	8.71
8	2.83	7	66	9.42
10	3.17	7	70	10
12	3.46	7	70	10
16	4	7	77	11

1b

$[CH_3COOH]$ (mM)	$[CH_3COOH]^{1/2}$ $(mM)^{1/2}$	i_p (μA)	i_c (μA)	i_c/i_p
1	1	6	24	4
2	1.41	6	36	6
3	1.73	6	40	6.67
4	2	6	45	7.50
6	2.45	6	49	8.17
8	2.83	6	53	8.83
10	3.16	6	54	9
12	3.46	6	56	9.33
16	4	6	56	9.33
20	4.47	6	59	9.83

2a

$[CH_3COOH]$ (mM)	$[CH_3COOH]^{1/2}$ $(mM)^{1/2}$	i_p (μA)	i_c (μA)	i_c/i_p
1	1	10	22	2.2
2	1.41	10	49	4.9
3	1.73	10	61	6.1
5	2.23	10	70	7
8	2.82	10	96	9.6
10	3.16	10	110	11
12	3.46	10	126	12.6
16	4	10	149	14.9
20	4.47	10	156	15.6
30	5.48	10	225	22.5
40	6.32	10	273	27.3
50	7.07	10	331	33.1
60	7.74	10	378	37.8
70	8.37	10	423	42.3
80	8.94	10	423	42.3

2b

$[CH_3COOH]$ (mM)	$[CH_3COOH]^{1/2}$ $(mM)^{1/2}$	i_p (μA)	i_c (μA)	i_c/i_p
1	1	9	38	4.22
2	1.41	9	46	5.11
4	2	9	59	6.56
6	2.45	9	70	7.78
8	2.83	9	84	9.33
10	3.16	9	99	11
20	4.47	9	149	16.56
30	5.48	9	203	22.56

40	6.32	9	249	27.67
60	7.75	9	356	39.56
80	8.94	9	451	50.11
120	10.95	9	625	69.44

References

[1] V.S. Thoi, N. Kornienko, C.G. Margarit, P. Yang, C.J. Chang, J. *Am. Chem. Soc.* 2013, 135, 14413-14424.

[2] Q.-X. Liu, Z.-Q. Yao, X.-J. Zhao, Z.-X. Zhao, X.-G. Wang, *Organometallics* 2013, 32, 3493-3501.

APPENDIX IV

Supplementary information on Chapter 4

*Table AIV.1. Crystallographic and structure refinement data for the complexes [Ni(**L1**)$_2$]Br$_2$ and [Ni(**L2**)$_2$]Br$_2$.*

	[Ni(**L1**)$_2$]Br$_2$	[Ni(**L2**)$_2$]Br$_2$
Empirical formula	$C_{40}H_{34}N_6Ni\cdot 2(Br)\cdot 0.904(H_2O)\cdot 0.416(O)$	$2(C_{38}H_{32}N_8Ni)\cdot 4(Br)\ CH_2Cl_2\cdot 4.184(O)\cdot 3(H_2O)$
Formula weight	840.16	1844.38
Temperature (K)	110(2)	110(2)
Crystal system	Triclinic	Monoclinic
Space group	*P*−*1*	*Cc*
a (Å)	11.5677 (3)	33.1815 (6)
b (Å)	16.6345 (4)	10.5397 (2)
c (Å)	19.7170 (6)	22.6091 (5)
α (°)	108.593 (2),	90
β (°)	93.914 (2)	95.2398 (18)
γ (°)	100.426 (2)	90
V (Å^3)	3504.17 (17)	7873.9 (3)
Z	4	4
D_{calc} (g/cm^3)	1.593	1.556
μ (mm^{-1})	2.88	2.64
F (000)	1705	3734
Crystal size (mm)	0.22 × 0.08 × 0.05	0.60 × 0.50 × 0.31
No. of measured, independent and observed [$I > 2\sigma(I)$] reflections	47791, 16092, 12186	51937, 17652, 16325
R-factor, $I > 2\sigma(I)$	$R_1 = 0.0387$, $wR_2 = 0.0830$	$R_1 = 0.0345$, $wR_2 = 0.0794$
R-factor (all data)	$R_1 = 0.0611$, $wR_2 = 0.0915$	$R_1 = 0.0394$, $wR_2 = 0.0818$
$\Delta\rho_{max}$, $\Delta\rho_{min}$ (e Å^{-3})	1.03, −0.57	1.16, −0.55

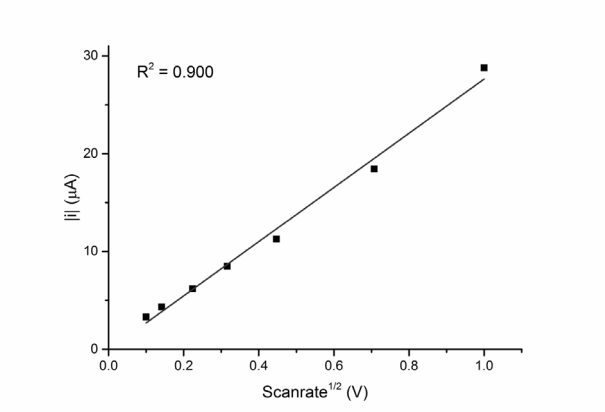

Figure AIV.1. Plots of reductive current i_{pc} vs. the square root of the scan rate for [Ni(**L1**)$_2$]Br$_2$ in DMF containing 0.1 M TBAP as supporting electrolyte at different at E_{pc} = −1.04 V, using a glassy carbon working electrode.

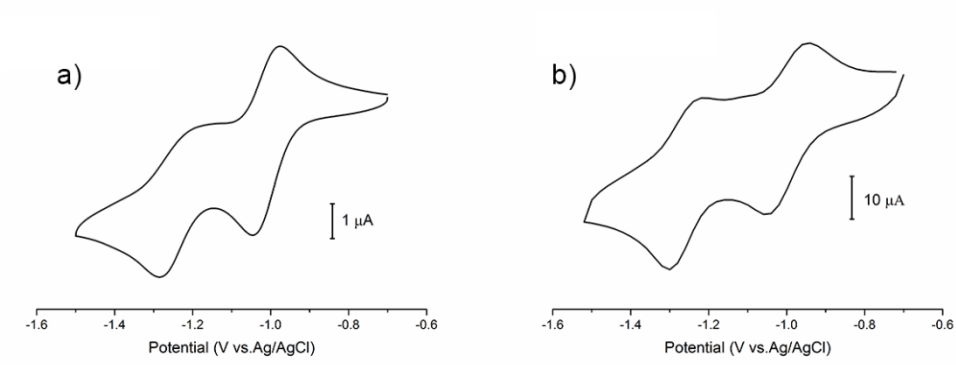

*Figure AIV.2. CVs of [Ni(**L1**)$_2$]Br$_2$ 1 mM in DMF containing 0.1 M TBAP as supporting electrolyte at different scan rate: (a) 10 mV/s; (b) 500 mV/s, using a glassy carbon working electrode.*

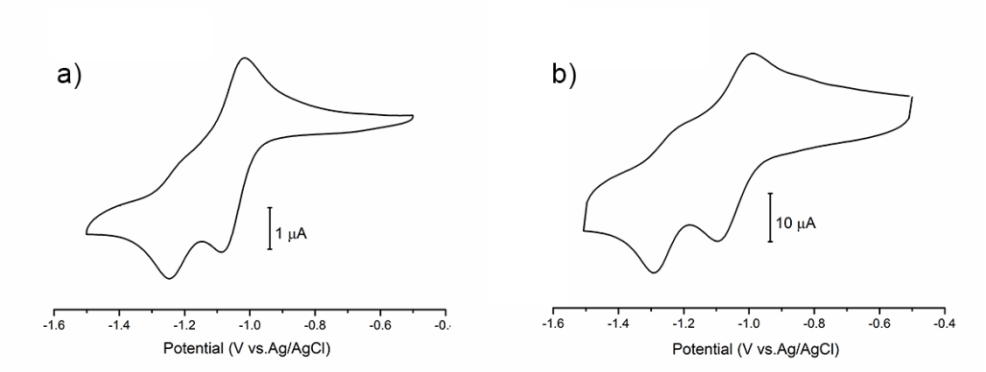

*Figure AIV.3. CV of [Ni(**L2**)$_2$]Br$_2$ in DMF containing 0.1 M TBAP as supporting electrolyte at different scan rate: (a) 10 mV/s; (b) 500 mV/s, using glassy carbon working electrode.*

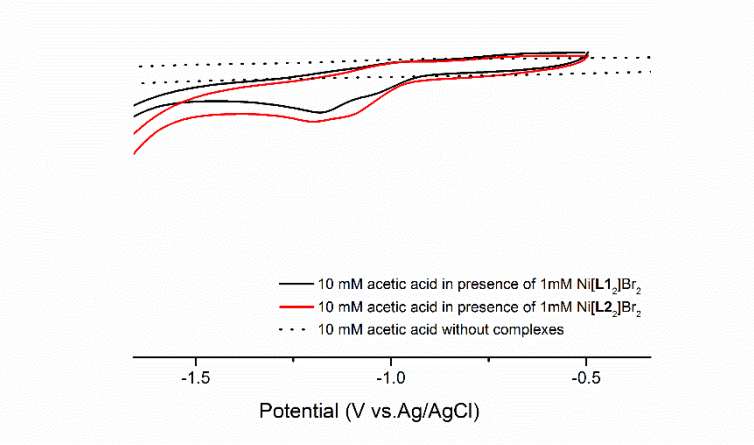

*Figure AIV.4. Zoom of CVs of complexes [Ni(**L1**)$_2$]Br$_2$ and [Ni(**L2**)$_2$]Br$_2$ in presence of 10 mM acetic acid in DMF containing 0.1 M TBAP as supporting electrolyte at scan rate 0.1 V/s, using a glassy carbon working electrode.*

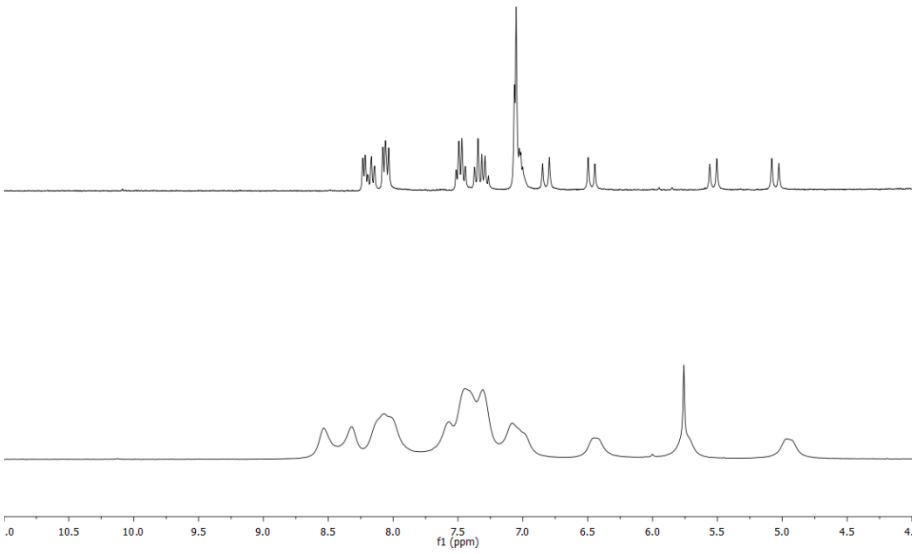

*Figure AIV.5. ^{1}H NMR spectra of complex [Ni(**L1**)$_2$]Br$_2$ (top) and [Ni(**L2**)$_2$]Br$_2$ (bottom) in DMSO-d$_6$.*

APPENDIX V

Supplementary information on Chapter 5

*Table AV.1. Selected crystallographic and structure refinement data for complexes [Ni(**L1**)]Cl and [Ni(**L2**)]PF_6.*

	[Ni(**L1**)]Cl	[Ni(**L2**)]PF_6
Empirical formula	$C_{17}H_{16}N_5NiO$,(Cl), 2.858(H_2O), 0.142(O)	$C_{21}H_{18}N_5NiO$, PF_6
Formula weight	454.27	560.08
Temperature (K)	110(2)	110(2)
Crystal system	monoclinic	triclinic
Space group	P $2_1/c$	P-1
a (Å)	9.4516(3)	7.1151(3)
b (Å)	14.7691(3)	11.9382(5)
c (Å)	13.4335(3)	12.9537(5)
α (°)	90	94.498(3)
β (°)	100.847(3)	97.028(3)
γ (°)	90	106.050(4)
V ($Å^3$)	1841.70(8)	1042.18(8)
Z	4	2
D_{calc} (g/cm^3)	1.638	1.785
μ (mm^{-1})	3.176	2.82
F (000)	943	568
Crystal size (mm)	0.17 × 0.11 × 0.01	0.24 × 0.13 × 0.05
No. of measured, independent and observed [$I > 2\sigma(I)$] reflections	10101, 3295, 2629	13223, 4059, 3515
R-factor, I > 2σ(I)	$R_1 = 0.0414$, $wR_2 = 0.1130$	$R_1 = 0.0320$, $wR_2 = 0.0777$
R-factor (all data)	$R_1 = 0.0572$, $wR_2 = 0.1030$	$R_1 = 0.0393$, $wR_2 = 0.0817$
$\Delta\rho_{max}$, $\Delta\rho_{min}$ (e $Å^{-3}$)	0.52, −0.70	0.57, −0.35

*Table AV.2. Selected bond distances (Å) and angles (°) of compounds [Ni(**L1**)]Cl and [Ni(**L2**)]PF_6.*

bond distances (Å)	[Ni(**L1**)]Cl	[Ni(**L2**)]PF_6	angles (°)	[Ni(**L1**)]Cl	[Ni(**L2**)]PF_6
Ni1–C12	1.832(3)	1.835(2)	C12-Ni1-N31	90.8(1)	89.95(8)
Ni1–N31	1.873(3)	1.856(2)	C12-Ni1-N22	89.3(1)	89.87(8)
Ni1–N42	1.936(2)	1.940(2)	C12-Ni1-N42	164.9(1)	162.96(8)
Ni1–N22	1.918(2)	1.918(2)	N31-Ni1-N22	169.3(1)	170.82(7)
C12–N13	1.336(4)	1.343(3)	N31-Ni1-N42	85.8(1)	85.62(7)
C12–N11	1.351(4)	1.349(2)	N22-Ni1-N42	96.8(1)	97.09(7)
C33–N31	1.313(4)	1.339(3)			
C33–O32	1.259(4)	1.247(3)			

*Table AV.3. Hydrogen bond list for compound [Ni(**L1**)]Cl.*

	D-H (Å)	H...A (Å)	D...A (Å)	<(DHA) (°)
O1W-H1W1...O32	0.82(2)	2.03(3)	2.847(3)	169(4)
O1W-H1W2...O32	0.84(2)	1.99(3)	2.822(3)	171(4)
O2W_a-H2W1_a...Cl1	0.89(3)	2.24(3)	3.123(4)	171(6)
O2W_a-H2W2_a...O3W_a	0.86(3)	2.28(8)	2.781(6)	117(7)
O2W'_b-H2W3_b...Cl1	0.84(3)	2.60(10)	3.353(11)	149(17)
O2W'_b-H2W4_b...Cl1	0.84(3)	2.66(5)	3.489(11)	167(16)
O3W_a-H3W1_a...O32	0.95(3)	1.90(3)	2.841(4)	170(6)
O3W_a-H3W2_a...Cl1	0.95(3)	2.05(3)	3.004(4)	175(5)

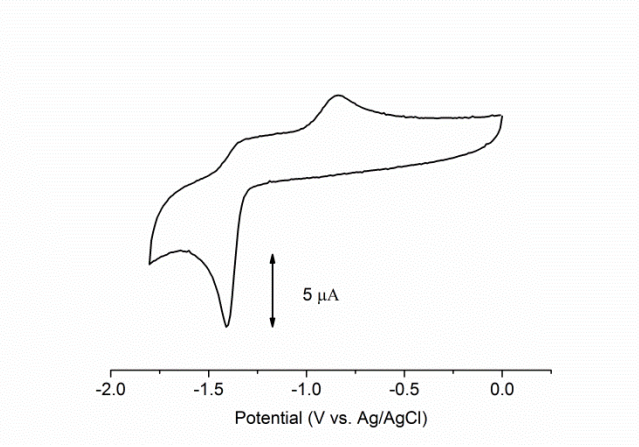

*Figure AV.1. Cyclic voltammogram of [Ni(**L1**)]Cl (1mM) recorded in DMF containing 0.1 M TBAP at scan rate 0.1 V/s, using a glassy carbon working electrode.*

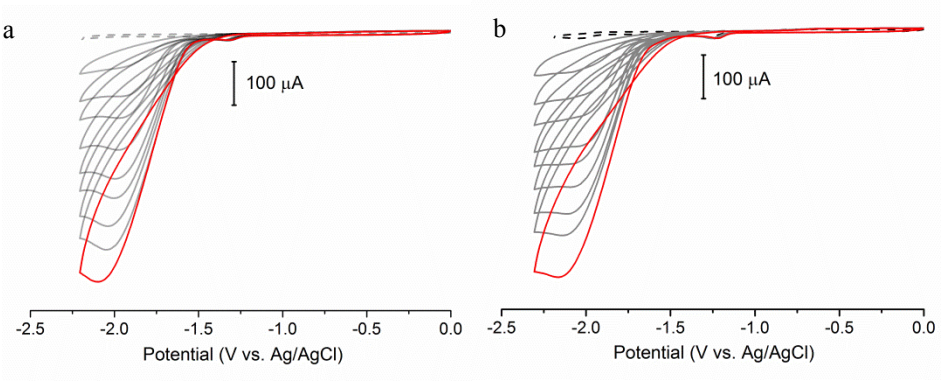

*Figure AV.2. CVs of 1 mM complex [Ni(**L1**)]Cl (a) and [Ni(**L2**)]PF_6 (b) in presence of various acid concentrations (0 − 100 mM) in. DMF containing 0.1 M TBAP as supporting electrode at a scan rate of 0.1 V/s, using a glassy carbon working electrode.*

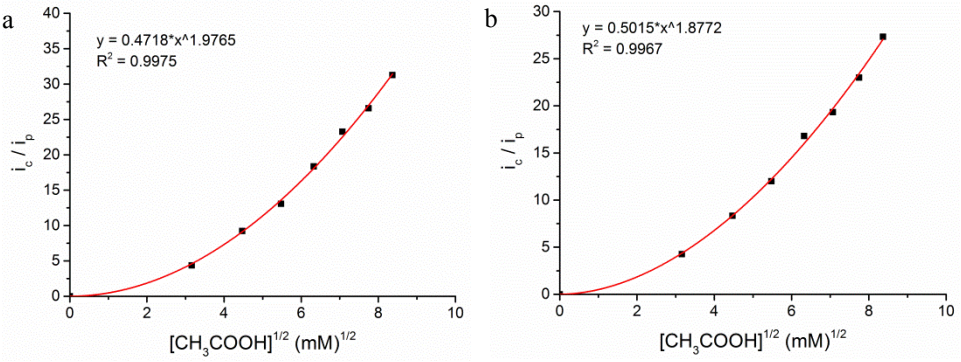

Figure AV.3. Plot of i_c/i_p vs. $[CH_3COOH]^{1/2}$ $(mM)^{1/2}$ for [Ni(**L1**)]Cl (a) and [Ni(**L2**)]PF_6 (b) in presence of various acid concentration in DMF containing 0.1 M TBAP as supporting electrode at 0.1 V/s, using a glassy carbon working electrode.

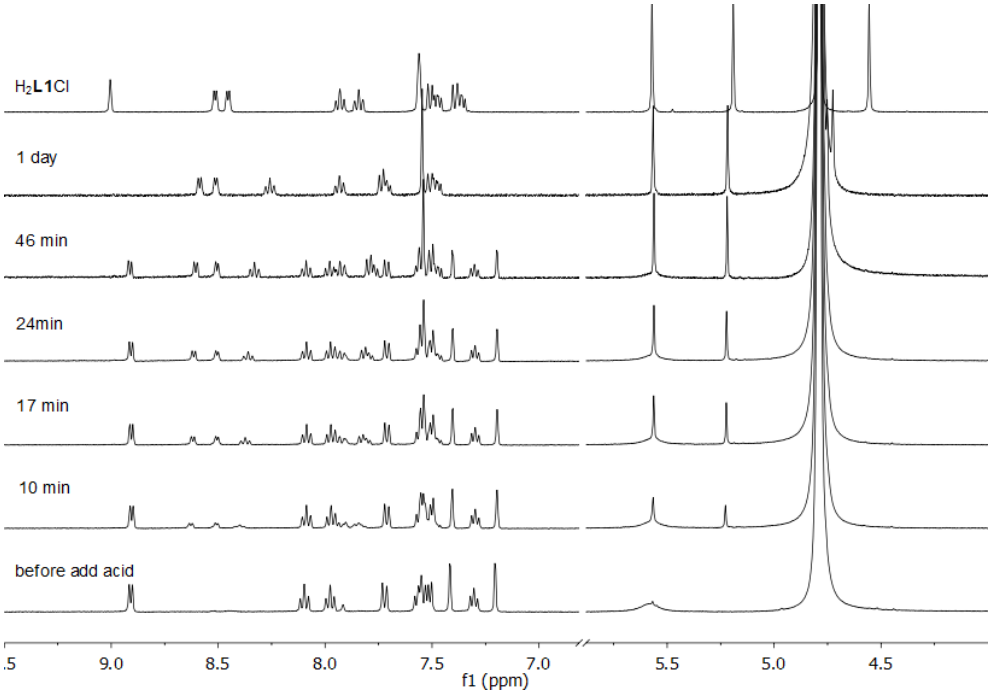

*Figure AV.4. ^{1}H NMR spectra of [Ni(**L1**)]Cl in D_2O in absence and in presence of acetic acid-d_4; ^{1}H NMR spectrum of ligand precursor H_2**L1**Cl is given at the top as comparison. Solvent residual signal set at 4.79 ppm for D_2O. After 1 day the chemical shift of decomposed complex shows slightly difference with the chemical shift of ligand precursor, probably due to the protonation of pyridine and amide group in acid environment.*

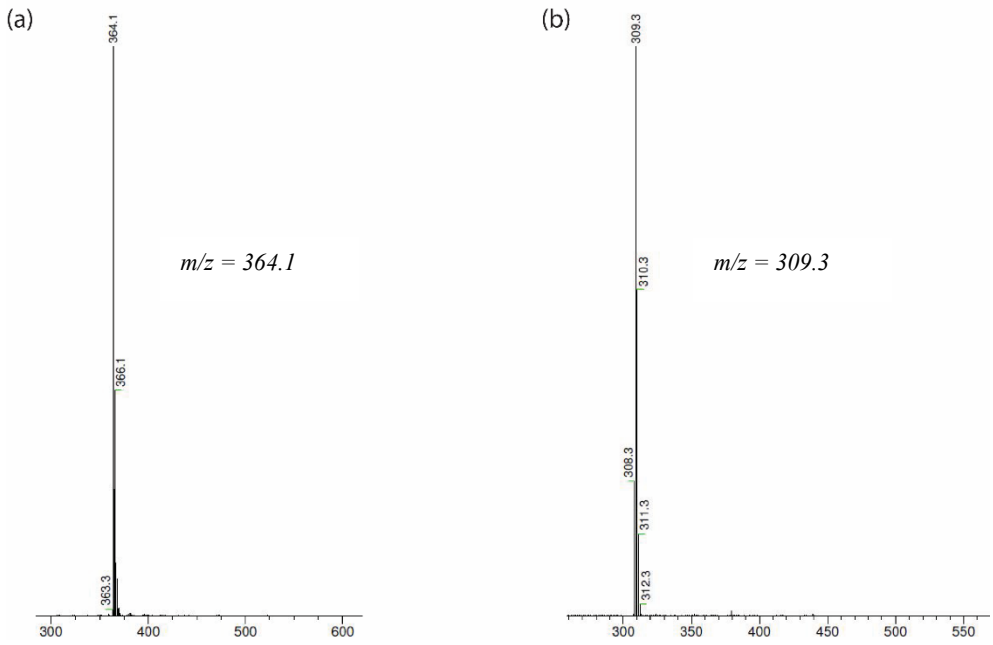

*Figure AV.5. Mass spectra of compound [Ni**L1**]Cl in D_2O before (a) and after (b) addition of acetic acid-d_4. Calculated for $[Ni\mathbf{L1}]^+$ m/z 364.07;calculated for $[HD\mathbf{L1}]^+$ m/z 309.16.*

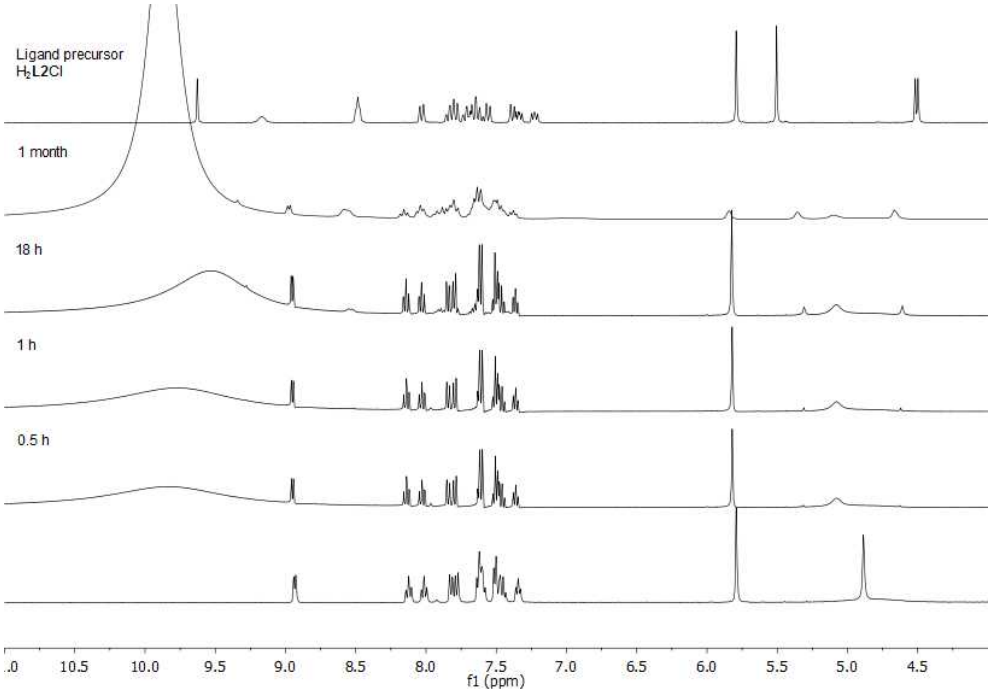

*Figure AV.6. ^1H NMR spectra of [Ni(**L2**)]PF_6 in acetonitrile-d_3 in absence (bottom) and presence of acetic acid-d_4; ^1H NMR spectrum of ligand precursor is given at the top as comparison.*

Table AV.4. Raw data for Figure 5.6 and Figure AV.3.

*[Ni(**L1**)]Cl*

$[CH_3COOH]$ (mM)	$[CH_3COOH]^{1/2}$ $(mM)^{1/2}$	i_p (μA)	i_c (μA)	i_c/i_p
10	3.16	14	61	4.36
20	4.47	14	129	9.21
30	5.48	14	183	13.07
40	6.32	14	257	18.36
50	7.07	14	326	23.29
60	7.76	14	372	26.57
70	8.37	14	438	31.29
80	8.94	14	493	35.21

*[Ni(**L2**)]PF_6*

$[CH_3COOH]$ (mM)	$[CH_3COOH]^{1/2}$ $(mM)^{1/2}$	i_p (μA)	i_c (μA)	i_c/i_p
10	3.16	15	64	4.27
20	4.47	15	125	8.33
30	5.48	15	180	12
40	6.32	15	252	16.8
50	7.07	15	290	19.33

60	7.75	15	347	23.13
70	8.37	15	410	27.33
80	8.94	15	461	30.73

Table AV.5. Raw data for Figure 5.7.

Scan rate (V/s)	i_c (μA)
0.05	630
0.1	751
0.2	1058
0.3	1354
0.5	1560
1	1987
2	2356

APPENDIX VI

Supplementary information on Chapter 6

*Table AVI.1. Selected crystallographic and structure refinement data for complexes [Co(**L2**)$_2$]Cl.*

	[Co(**L2**)$_2$]Cl
Empirical formula	$2(C_{34}H_{32}CoN_{10}O_2)\cdot 5(H_2O)\cdot 2(Cl)$
Formula weight	1504.23
Temperature (K)	110(2)
Crystal system	monoclinic
Space group	P $2_1/n$
a (Å)	13.5141(3)
b (Å)	16.3049(4)
c (Å)	15.5444(4)
α (°)	90
β (°)	105.250 (2)
γ (°)	90
V (Å^3)	3304.54 (14)
Z	2
D_{calc} (g/cm^3)	1.638
μ (mm^{-1})	0.66
F (000)	943
Crystal size (mm)	0.27 × 0.24 × 0.13
No. of measured, independent and observed [$I > 2\sigma(I)$] reflections	25481, 10320, 7559
R-factor, I > 2σ(I)	$R_1 = 0.0396$, $wR_2 = 0.1003$
R-factor (all data)	$R_1 = 0.0544$, $wR_2 = 0.0915$
$\Delta\rho_{max}$, $\Delta\rho_{min}$ (e Å^{-3})	0.63, −0.53

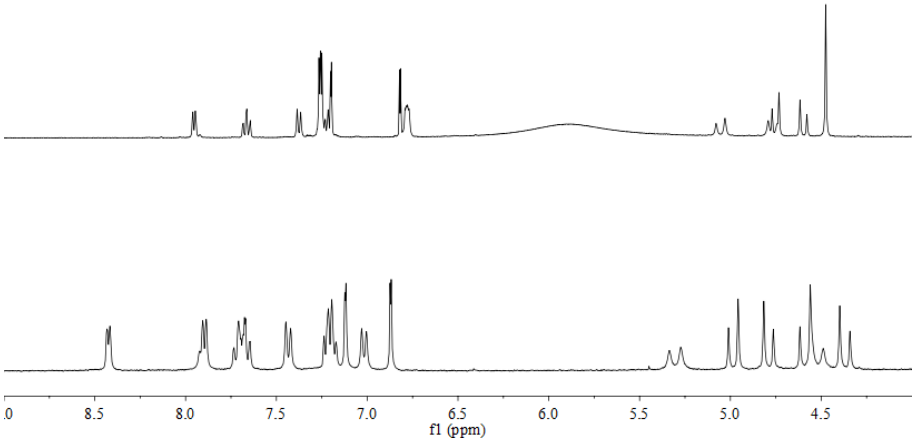

*Figure AVI.1. ^{1}H NMR spectra of complex [Co(**L1**)$_2$]Cl (top) and [Co(**L2**)$_2$]Cl (bottom) in acetonitrile-d_3.*

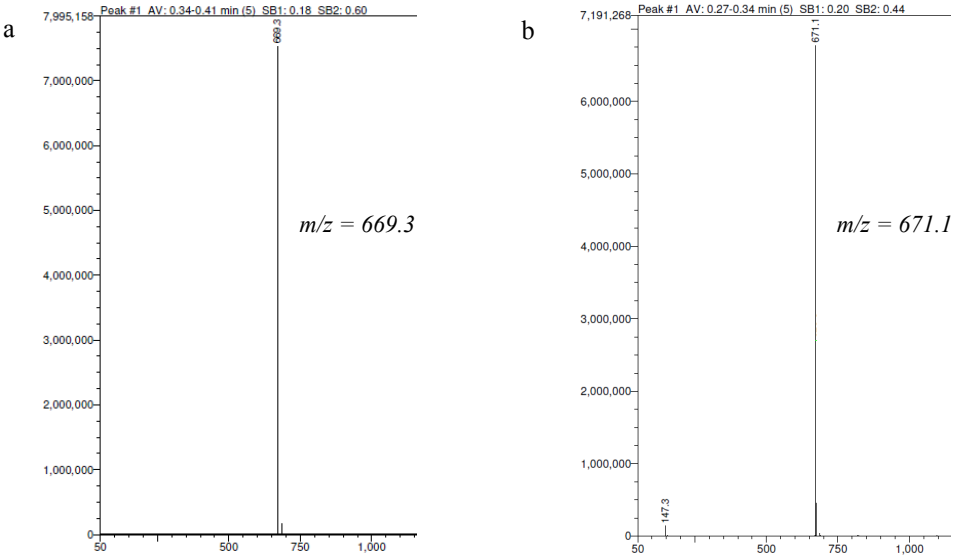

*Figure AVI.2. ESI-MS spectra of complex (a) [Co(**L1**)$_2$]Cl (calculated $[M–Cl]^+$ m/z 669.21) and (b) [Co(**L2**)$_2$]Cl (calculated $[M–Cl]^+$ m/z 671.2).*

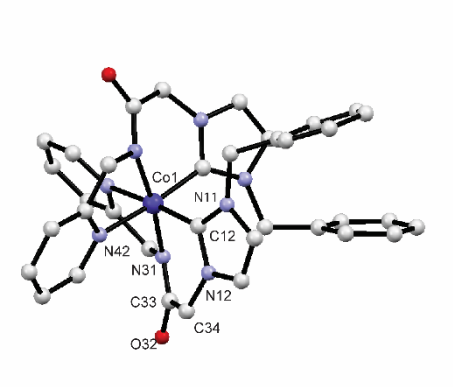

*Figure AVI.3. Ball and stick projection of the cationic complex in [Co(**L1**)$_2$]PF$_6$ with selected labeling. The counter ions could not be located due to disorder.*

*Table AVI.2. Selected bond distances (Å) and angles (°) of compounds [Co(**L1**)$_2$]PF$_6$ and [Co(**L2**)$_2$]Cl.*

	[Co(**L1**)$_2$]PF$_6$	[Co(**L2**)$_2$]Cl
Co1–C12A	1.9067	1.917(2)
Co1–N31A	1.9023	1.9236(17)
Co1–N42A	2.0087	1.9867(18)
C12B-Co1-N31A	93.25	93.66(8)
C12A-Co1-N31A	91.97	89.84(8)
N31B-Co1-N42A	92.79	96.8(12)
N31A-Co1-N42A	81.99	81.53(7)
C12B-Co1-C12A	88.29	88.01(9)
N42B-Co1-N42A	88.68	86.56(7)
C12B-Co1-N42A	91.83	92.54(8)
C12A-Co1-N42A	173.95	171.37(8)
C12B-Co1-N42B	173.95	171.53(8)
N31A-Co1-N31B	172.72	174.10

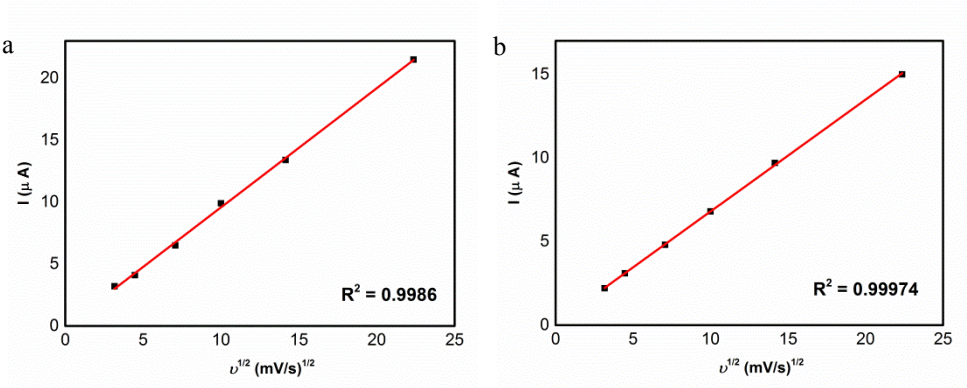

*Figure AVI.4. Plots of reductive current vs. the square root of the scan rate of [Co(**L1**)$_2$]Cl (a) and [Co(**L2**)$_2$]Cl **(b)** in DMF both at E = −1.22 V vs. Ag/AgCl, respectively.*

*Redox properties of H$_2$**L1**Cl and H$_2$**L2**Cl*

The redox properties of the ligand precursors were also investigated. Both the precursors H$_2$**L1**Cl and H$_2$**L2**Cl show an irreversible reduction at around −2 V (for H$_2$**L1**Cl at −2.03 V and H$_2$**L2**Cl at −2.15 V) (Figure AVI.5). In addition, CVs of two ligand precursors were recorded in the presence of various concentrations of acetic acid (from 10 mM to 40 mM). For both ligand precursors a new irreversible reductive current response is observed at around −1.84 V. This catalytic current response was observed before the reduction of ligand (Figure AVI.5). The catalytic current remained steady and stopped to increase at a certain concentration of acid (10 mM for H$_2$**L1**Cl and 20 mM for H$_2$**L2**Cl). In presence of 40 mM acetic acid, compared to H$_2$**L1**Cl, the catalytic current of H$_2$**L2**Cl is doubled. Although without metal center, both ligand precursors show weak catalytic activity on HER. But the catalytic activity of H$_2$**L2**Cl is faster than its partner. Considering the structure difference between two ligand precursors (H$_2$**L2**Cl contains two pyridine group but H$_2$**L1**Cl only contains one), we assume that the pyridine group takes part into the electrocatalytic cycle.

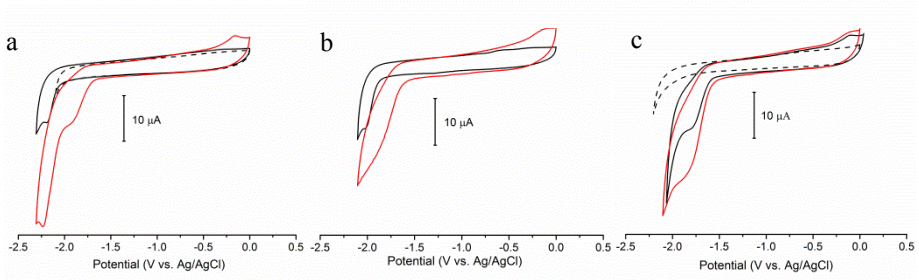

*Figure AVI.5. CVs of ligand precursors H$_2$**L1**Cl (1 mM) and H$_2$**L2**Cl (1 mM) in absence and in presence of acid: (a) CVs of H$_2$**L1**Cl in absence of acid (solid black line in the range 0 to −2.3 V; black dashed line in the range 0 to −2.1 V) and in presence of 10 mM acetic acid (solid red line); (b) CVs of H$_2$**L2**Cl in absence of acid (solid black line) and in presence of 10 mM acetic acid (solid red line); (c) CVs of H$_2$**L1**Cl (1 mM) (solid black line) and H$_2$**L2**Cl (1 mM) (solid red line) in presence of 40 mM acetic acid (black dashed line).*

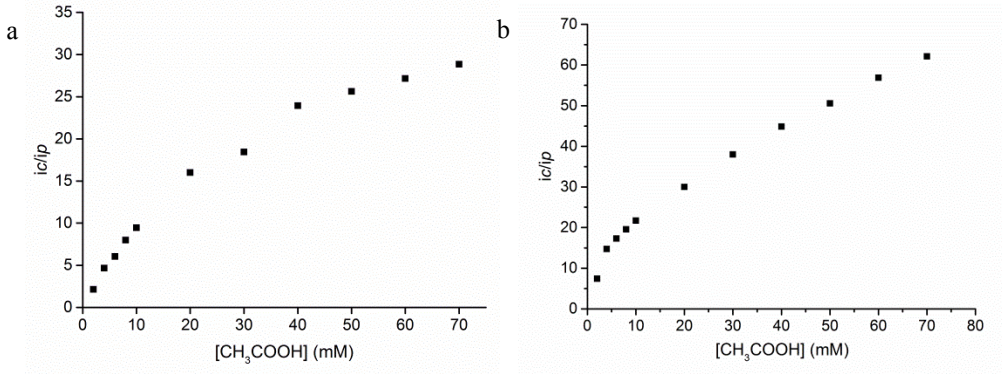

*Figure AVI.6. Plot of i_c/i_p vs. [CH_3COOH] (mM) for [Co(**L1**)$_2$]Cl (a) and [Co(**L2**)$_2$]Cl (b), measured in presence of various acid concentration in DMF containing 0.1 M TBAP as supporting electrode at 0.1 V/s, using glassy carbon working electrode.*

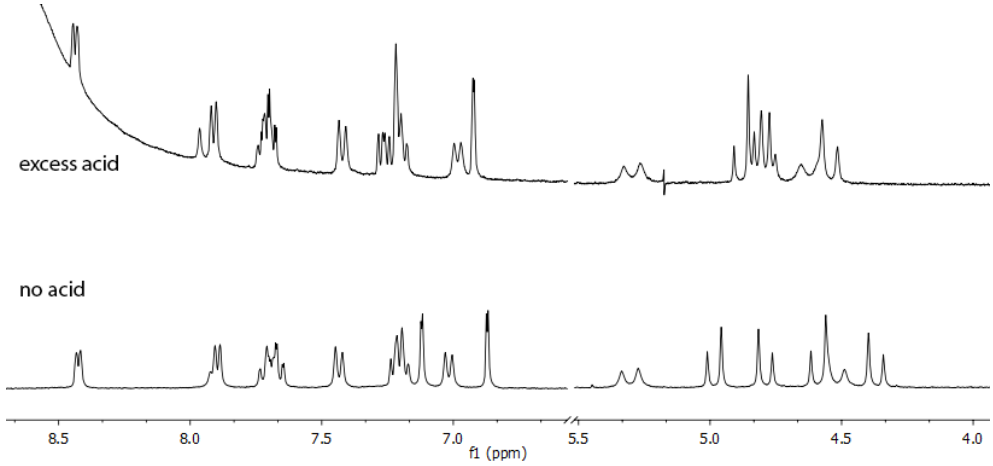

*Figure AVI.7. ^1H NMR spectra of [Co(**L2**)$_2$]Cl in acetonitrile-d_3 in absence or presence of acetic acid-d_4. The peaks shifted downfield in presence of acid probably due to the protonation of the free pyridine group. The protonation can be confirmed by the EI-MS spectrum of the sample after NMR measurement (Figure AVI.8).*

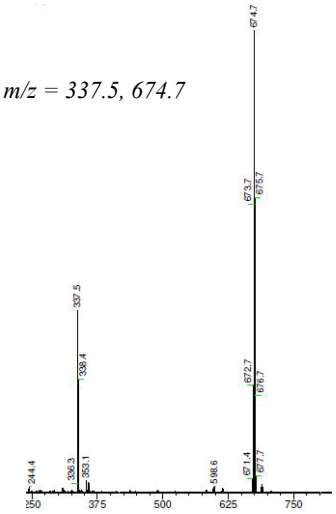

*Figure AVI.8. Mass spectra of compound [Co(**L2**)$_2$]Cl in acetonitrile-d$_3$ in prence of acetic acid-d$_4$. Calculated for [Co(**L2**D)$_2$]$^{2+}$ m/z 337.6;calculated for [Co(**L2**)(**L2**D)]$^+$ m/z 673.22.*

Table AVI.2. Raw data for Figure 6.7, Figure 6.8 and Figure AVI.6.

*[Co(**L1**)$_2$]Cl*

[CH_3COOH] (mM)	[CH_3COOH]$^{1/2}$ (mM)$^{1/2}$	i_p (μA)	i_c (μA)	i_c/i_p	k_{obs} (s^{-1})
2	1.41	11	26	2.36	0.90
4	2	11	54	4.91	4.23
6	2.45	11	67	6.09	7.07
8	2.83	11	87	7.91	12.39
10	3.16	11	102	9.27	17.30
20	4.47	11	177	16.09	49.72
30	5.48	11	203	18.45	66.06
40	6.32	11	261	23.73	111.22
50	7.07	11	279	25.36	127.36
60	7.75	11	294	26.73	143.11
70	8.37	11	313	28.45	161.46

*[Co(**L2**)$_2$]Cl*

[CH_3COOH] (mM)	[CH_3COOH]$^{1/2}$ (mM)$^{1/2}$	i_p (μA)	i_c (μA)	i_c/i_p	k_{obs} (s^{-1})
2	1.41	7	52	7.43	10.71
4	2	7	103	14.71	42.00
6	2.45	7	121	17.29	57.97
8	2.83	7	137	19.57	74.31
10	3.16	7	152	21.71	91.47
20	4.47	7	210	30	174.6
30	5.48	7	266	38	280.17
40	6.32	7	314	44.86	390.36
50	7.07	7	354	50.57	496.15
60	7.75	7	398	56.86	627.15
70	8.37	7	435	62.14	749.18